

# The impact of individual nuclear masses on $r$ -process abundances

M.R. Mumpower<sup>1,2</sup>, R. Surman<sup>1,2</sup>, D.-L. Fang<sup>2,3</sup>, M. Beard<sup>1,2</sup>, P. Möller<sup>4</sup>, T. Kawano<sup>4</sup>, and A. Aprahamian<sup>1,2</sup>

<sup>1</sup>*Department of Physics, University of Notre Dame, Notre Dame, Indiana 46556, USA*

<sup>2</sup>*Joint Institute for Nuclear Astrophysics, USA*

<sup>3</sup>*Department of Physics, Michigan State University, East Lansing, MI 48824, USA and*

<sup>4</sup>*Theoretical Division, Los Alamos National Laboratory, Los Alamos, New Mexico 87545, USA*

(Dated: November 13, 2018)

We have performed for the first time a comprehensive study of the sensitivity of  $r$ -process nucleosynthesis to individual nuclear masses across the chart of nuclides. Using the latest version (2012) of the Finite-Range Droplet Model, we consider mass variations of  $\pm 0.5$  MeV and propagate each mass change to all affected quantities, including  $Q$ -values, reaction rates, and branching ratios. We find such mass variations can result in up to an order of magnitude local change in the final abundance pattern produced in an  $r$ -process simulation. We identify key nuclei whose masses have a substantial impact on abundance predictions for hot, cold, and neutron star merger  $r$ -process scenarios and could be measured at future radioactive beam facilities.

PACS numbers: 21.10.Dr, 26.30.Hj, 25.20.-x, 26.30.-k

## I. INTRODUCTION

One of the most challenging open questions in all of physics is the identification of the site or sites of rapid neutron capture, or  $r$ -process, nucleosynthesis [1, 2]. Production of the heaviest  $r$ -process elements requires on the order of 100 neutron captures per seed nucleus; exactly where and how such rapid neutron captures occur has yet to be definitively determined [3].

One attractive potential site is within the cold or mildly heated tidal ejecta from neutron star or neutron star-black hole mergers [4]. Current state-of-the-art simulations show a vigorous  $r$  process with fission recycling in the merger ejecta [5–8]. The resulting abundance pattern is relatively insensitive to variations in the initial conditions, which naturally explains the consistent  $56 < Z < 82$  pattern observed in the solar system and  $r$ -process-enhanced halo stars [9, 10]. Vigorous production of radioactive  $r$ -process nuclei can also lead to an observable electromagnetic transient accompanying the merger event [11–13], an example of which may have already been detected [14, 15]. It is less clear whether mergers happen often enough or early enough in galactic history to fit all of the observational data [16–18]. The neutrino-driven wind within a core-collapse supernova is perhaps the best-studied alternative [19, 20], though the combination of moderate neutron-richness, high entropy, and fast outflow timescale required to make the heaviest  $r$ -process elements does not appear to be achieved in modern simulations [21–24]. Instead attention has shifted to more exotic sites connected to the deaths of massive stars, including neutron-rich jets [25], supernova neutrino-induced nucleosynthesis in the helium shell [26], and collapsar outflows [27, 28].

In principle, the proposed environments have such distinct astrophysical conditions that their abundance pattern predictions should be clearly distinguishable. Currently simulations lack this precision [29, 30], in large part due to uncertainties in the required nuclear data. Proper-

ties such as masses, neutron capture rates,  $\beta$ -decay rates, and  $\beta$ -delayed neutron emission probabilities are needed for thousands of neutron-rich nuclear species from the valley of stability to the neutron drip line. Presently there is little experimental information available for the vast majority of these quantities. Simulations must instead rely on extrapolated or theoretical values, where different approaches can produce markedly different (and often divergent) predictions.

Nuclear masses are particularly important for the  $r$  process as they enter into the calculations of all of the aforementioned nuclear properties, which shape how each phase of the  $r$  process proceeds. In a classic  $r$  process, an equilibrium is established between neutron captures and photodissociations, and nuclear masses directly determine the  $r$ -process path through a Saha equation:

$$\frac{Y(Z, N+1)}{Y(Z, N)} \propto \frac{G(Z, N+1)}{2G(Z, N)} \frac{N_n}{(kT)^{3/2}} \exp \left[ \frac{S_n(Z, N+1)}{kT} \right] \quad (1)$$

where  $G(Z, N)$  are the partition functions,  $N_n$  is the neutron number density,  $kT$  is the temperature in MeV, and  $S_n(Z, N+1)$  is the neutron separation energy, the difference in binding energy between the nuclei  $(Z, N+1)$  and  $(Z, N)$ . Each isotopic chain is connected to its neighbors by  $\beta$ -decay, and thus the  $\beta$ -decay lifetimes of nuclei along the  $r$ -process path set their relative abundances. Modern nuclear network calculations show that this equilibrium picture is an excellent approximation for early-time  $r$ -process evolution in many astrophysical scenarios. Eventually  $(n, \gamma) \rightleftharpoons (\gamma, n)$  equilibrium fails, or in some scenarios is not established at all, and then neutron capture, photodissociation, and  $\beta$ -decay all compete to shape the final abundance pattern.

The roles of these individual pieces of data in  $r$ -process nuclear network simulations have been examined via sensitivity studies. In these studies, baseline astrophysical conditions are chosen, a single nuclear property is varied, and the simulation is rerun with the nuclear data change and compared to the baseline. Sensitivity stud-

ies highlight the pieces of data with the most leverage on the final abundance pattern and elucidate the mechanisms of influence. They have so far been performed for neutron capture rates [31–34],  $\beta$ -decay rates [34, 35], and photodissociation rates via their dependence on nuclear masses [36–38], and are in progress for  $\beta$ -delayed neutron emission probabilities [39]. These studies are distinct from and complementary to studies of the influence of groups of nuclear properties, e.g. [40, 41], global theoretical model predictions, e.g. [42], or global variations in a Monte Carlo approach [29, 30] that can quantify correlations between nuclear physics inputs [43].

The sensitivity studies described above looked for the individual nuclear properties with the greatest impact on the  $r$  process by considering variations of one piece of data at a time. However, we know that modifying a single nuclear mass alters all of the nuclear properties that depend on that mass. Here we perform nuclear mass  $r$ -process sensitivity studies in which variations in individual nuclear masses are consistently propagated to all affected nuclear properties, including neutron capture rates, photodissociation rates, and  $\beta$ -decay properties. This approach was developed in Ref. [44] for spherical nuclei and is extended for the first time in this work to the entire chart of the nuclides between  $Z = 30$  and  $Z = 80$ . These new studies capture the full impact of the uncertainties in individual masses on the  $r$  process and point to the most important masses to measure in present and future experimental campaigns. Additionally they place direct constraints on the precision needed for measurements of nuclear properties and theoretical models, in order to improve  $r$ -process predictions and, eventually, distinguish between possible astrophysical sites.

## II. BASELINE $r$ -PROCESS SIMULATIONS

We begin our sensitivity studies with a choice of baseline astrophysical trajectories. We investigate a range of astrophysical conditions including a low entropy hot wind, high entropy hot wind, a cold wind and a neutron star merger. In a hot wind an equilibrium is established between neutron captures and their inverse reaction, photodissociation, and the  $\beta$ -decays that move the nuclear flow to higher atomic number,  $Z$ , control the timescale for heavy-element production. Nuclear masses are influential during equilibrium as they directly set the  $r$ -process path for a given temperature and density, as shown in Eqn. 1. To explore nuclear mass uncertainties in a low entropy hot wind we use a parameterized wind model from [45] which has an entropy of  $30 k_B$ , an electron fraction of  $Y_e = 0.20$  and a timescale of 70 ms. This trajectory yields the production of heavy elements out to the third peak but is not neutron rich enough to lead to fission recycling. The high entropy hot trajectory uses the same parameterization with entropy of  $100 k_B$ , an electron fraction of  $Y_e = 0.25$  and a timescale of 80 ms. In a cold wind the  $(n, \gamma) \rightleftharpoons (\gamma, n)$  equilibrium is short-

lived as the temperature drops quickly and photodissociation becomes negligible. The  $r$ -process path moves far from stability where a new quasi-equilibrium can be established between neutron captures and  $\beta$ -decays. To study nuclear masses under these conditions we employ a neutrino-driven wind simulation of Ref. [46] with artificially reduced electron fraction of  $Y_e = 0.31$  to produce a main  $r$  process. We also consider a neutron star merger environment using a trajectory from Bauswein and Janka, for which the mildly-heated ejecta is sufficiently neutron-rich to undergo fission recycling [5].

In all cases, once the supply of free neutrons is consumed the  $r$ -process path begins to move back to stability. The criterion of neutron exhaustion signals the start of the freeze-out phase of the  $r$  process in which key abundance features are formed, such as the rare earth peak [47, 48]. Additional neutrons during this time come from photodissociation, neutrons emitted promptly after  $\beta$ -decay, or fission [49]. During this freeze-out phase the reaction flows are sensitive to individual masses of nuclei between the  $r$ -process path and stability.

Our studies employ a dedicated  $r$ -process reaction network code [47, 50] which has been updated in recent studies [49, 51] and includes a schematic treatment of fission [52]. For the baseline nuclear masses we use the 2012 version of the Finite-Range Droplet Model (FRDM2012) [53]. This model has an root-mean-square (rms) error of 0.57 MeV compared to known masses from the Atomic Mass Evaluation (AME2012) [54]. When available, we use measured masses from the AME and keep these masses unchanged during our calculations. The use of experimental (AME2012) and theoretical (FRDM2012) mass values requires some care to avoid large discontinuities. Therefore when calculating quantities that depend on two masses of different origin (theory and experiment), we make sure to consistently calculate that quantity within a given dataset. For example, if a measured mass is available for  $(Z + 1, N - 1)$  but not  $(Z, N)$ , the  $\beta$ -decay  $Q$ -value for  $(Z, N)$  is calculated from the FRDM2012 masses only.

The baseline neutron capture rates are calculated with the publicly available statistical model code TALYS [55] using FRDM2012 and the latest compilation of measured masses from the AME2012 as described above. We use the default settings for level density,  $\gamma$ -strength function and particle optical model. The default level density model used in TALYS combines a constant nuclear temperature at low energies and matches it with a back-shifted Fermi gas model using systematics [56]. Masses can enter into this level density model via the definition of the constant temperature, which, as used in the TALYS code, is proportional to one over the square root of the shell correction term:  $dW(Z, N) = M(Z, N) - M_{LDM}(Z, N)$  where  $M(Z, N)$  is the mass of the nucleus and  $M_{LDM}(Z, N)$  is the predicted mass to a spherical liquid-drop. Additionally, the level density parameter,  $a$ , is proportional to  $dW$  and hence the nuclear masses. The default  $\gamma$ -strength function used in

TALYS is the formulation set out in Kopecky-Uhl (KU) [57]. Nuclear masses enter into this parameterization of the giant dipole resonance via nuclear temperature term which prevents the  $\gamma$  strength from going to zero as  $\gamma$  energy decreases. The nuclear temperature itself is proportional to the square root of the neutron separation energy,  $S_n$ , as well as  $a$ , evaluated at  $S_n$ .

Photodissociation rates are calculated from neutron capture rates by detailed balance:

$$\lambda_\gamma(Z, N) \propto T^{3/2} \exp\left[-\frac{S_n(Z, N)}{kT}\right] \langle\sigma v\rangle_{(Z, N-1)} \quad (2)$$

where  $S_n(Z, N) = M(Z, N-1) - M(Z, N) + M_n$  is the one neutron separation energy,  $M(Z, N)$  and  $M(Z, N-1)$  are masses of the nuclides,  $M_n$  is the mass of the neutron,  $T$  is the temperature,  $\langle\sigma v\rangle_{(Z, N-1)}$  is the neutron capture rate of the neighboring nucleus and  $k$  is Boltzmann's constant. The baseline photodissociation rates use FRDM2012 & AME2012 masses and the neutron capture rates as calculated above.

For the baseline  $\beta$ -decay rates we use experimental values [58] where available and theoretical estimates everywhere else. Theoretical rates are calculated as in [59]:

$$\lambda_\beta \equiv \frac{\ln(2)}{t_{1/2}} = \sum_i f_{\omega_i}^I C^I(\omega_i) \quad (3)$$

where  $\lambda_\beta$  is the  $\beta$ -decay rate,  $t_{1/2}$  is the half-life,  $i$  denotes the  $i$ th excited state of the daughter nucleus with energy  $E_i$ ,  $\omega_i = (Q_\beta - E_i)/m_e$  is the  $\beta$ -decay energy to this state in units of electron mass,  $I$  is the type of the decay, either Gamow-Teller (GT) or First-Forbidden (FF),  $f$  is the phase space factor and  $C$  is the  $\beta$ -strength function. We use the  $\beta$ -decay strength data from [59] and calculate the phase space piece using FRDM2012 & AME2012 masses as described above. Neutron emission probabilities are calculated by combining the Quasiparticle Random-Phase Approximation (QRPA) model of Ref. [59] with a Hauser-Feshbach (HF) model from Ref. [60] which has been extended to the neutron dripline in this work. This combined QRPA-HF approach produces larger predictions of average neutron emission towards the dripline compared to older (QRPA) methods, as it follows the statistical decay until the initial available excitation energy is exhausted.

### III. MASS VARIATION PROPAGATION

For the sensitivity studies of this work we consider mass variations of  $\pm 0.5$  MeV, approximately equal to the rms error of FRDM2012. Since measured masses tend to have experimental uncertainties much smaller than this, we restrict our individual mass variations to nuclei with extrapolated or unknown masses.

When an uncertain nuclear mass is varied we **recalculate** all the relevant nuclear properties of neighboring nuclei that depend on the changed mass. Specifically, if

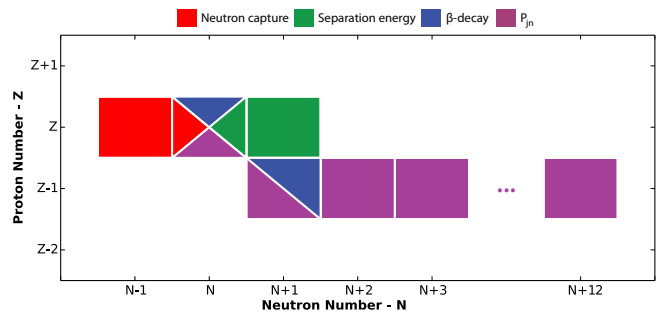


FIG. 1: Shows the quantities of neighboring nuclei of importance to the  $r$ -process that may be altered by a change in mass of nucleus with  $Z$  protons and  $N$  neutrons.

the mass of a nucleus ( $Z, N$ ) with  $Z$  protons and  $N$  neutrons is varied then it can lead to changes in the neutron capture rates of ( $Z, N$ ) and ( $Z, N-1$ ), the separation energies of ( $Z, N$ ) and ( $Z, N+1$ ), the  $\beta$ -decay rates of ( $Z, N$ ) and ( $Z-1, N+1$ ), and  $\beta$ -delayed neutron emission probabilities of ( $Z, N$ ), ( $Z-1, N+1$ ), ( $Z-1, N+2$ ), up to ( $Z-1, N+12$ ) as shown in Fig. 1.

To propagate the changes to the neighboring neutron capture rates we invoke the ‘massnucleus’ command in TALYS and continue to use the default settings for level density,  $\gamma$ -strength function and particle optical model with the varied mass. A  $\pm 0.5$  MeV mass variation results in a change in neutron capture rates of a factor of approximately two to five. Note that this corresponds to the uncertainty in the neutron capture rates due only to uncertain nuclear masses; larger variations in the rates come from choice of statistical model components and the treatment of direct capture [61]. The impact on the  $r$  process of these larger neutron capture rate uncertainties are addressed in earlier studies [32, 33, 50].

For the  $\beta$ -decay rates, all measured half-lives remain unchanged during our mass variations and we adjust only the affected theoretical rates. For the theoretical values, the majority of the dependence on nuclear mass is contained in the phase space piece, which goes as  $f(\omega) \sim \omega^5$  for allowed decays. This is a significantly stronger dependence on masses than appears in the nuclear matrix elements calculated in the QRPA [44]. Therefore when updating the theoretical rates with the mass variations we recalculate only the phase space factors and leave the  $\beta$ -strength functions unchanged. This greatly reduces the numerical cost of the calculation while still capturing most of the dependence of the half-lives on the masses. We find mass variations of  $\pm 0.5$  MeV lead to changes in the half-lives by a factor of roughly two to four.

We recalculate the affected  $\beta$ -delayed neutron branching ratios in our QRPA-HF approach, assuming the structure of the ground state does not change with the mass variation. Modifications come from a change in the  $\beta$ -decay  $Q$ -value of the parent nucleus or from a change to the neutron separation energies of the daughter nuclei.

A general dependence of neutron emission probabilities on changes in mass using QRPA-HF is thus entangled with the inclusion of  $\gamma$ -ray competition at each neutron emission stage.

#### IV. MASS SENSITIVITY STUDY

With the required baseline nuclear data generated as described in Sec. II and the computational tools in place to propagate the mass variations to the affected nuclear properties as described in Sec. III, we begin our sensitivity studies with the baseline astrophysical trajectories identified in Sec. II. For each nuclear species ( $Z, N$ ) we repeat the baseline  $r$ -process simulation twice: once where the mass  $M(Z, N)$  is increased by 0.5 MeV and once where the mass is decreased by 0.5 MeV. We then compute the metric

$$F = 100 \sum_A |X(A) - X_b(A)| \quad (4)$$

where  $X_b(A)$  is the final isobaric mass fraction in the baseline simulation,  $X(A)$  is the final isobaric mass fraction of the simulation when all nuclear inputs have been modified based off the change in a single mass, and the summation runs over the entire baseline pattern [44]. As defined here, the  $F$  metric quantifies the impact of the mass on the *global*  $r$ -process pattern. This procedure is then repeated for every nuclear species from the limits of the AME2012 experimental values to the FRDM2012 neutron drip line.

Fig. 2 shows the results of the full-chart mass sensitivity studies run for our four choices of astrophysical conditions. The shading of each rectangle represents the largest of the two  $F$  values that we obtained when we calculated the  $r$ -process abundances for the reference mass (FRDM2012) (1) plus 0.5 MeV and (2) minus 0.5 MeV. Roughly 1100 nuclei are included in each study with  $30 \leq Z \leq 80$  and  $60 \leq N \leq 130$ . As a general result, we find influential nuclear masses lie along the equilibrium  $r$ -process path as well as along the decay pathways back to stability, most of which are within the predicted experimental reach of the upcoming Facility for Rare Isotope Beams (FRIB) [62]. This is particularly evident around the closed neutron shells where we find the largest global impact of nuclear masses.

Qualitatively, the overall distribution of influential nuclear masses in the four cases reinforces the conclusions from our previous work [36, 38, 44]. In particular the pattern of most impactful nuclei for the hot wind  $r$  process shown in the top panel of Fig. 2 is directly comparable to that from [36, 38]. Our new studies show several key improvements, which come from addressing the limitations of these early studies. Refs. [36, 38] considered the propagation of mass variations to photodissociation rates only, which underestimates the resulting sensitivity measures, especially in cold wind or merger  $r$ -process scenarios where photodissociation is suppressed. In these

cases, the influence of masses on the  $r$  process occurs via the decay properties and neutron capture rates—an effect which was captured for the first time in Ref. [44] but only for closed shell nuclei. Thus our new studies are the first reliable full-chart estimates of the impact of nuclear masses in cold and merger  $r$ -process scenarios. In addition, the hot wind studies show higher mass sensitivities in the rare earth region compared to the earlier studies, due to the interplay of  $\beta$ -decay, neutron capture, and photodissociation that forms the rare earth peak [47, 49]. The exact mechanisms by which each piece of nuclear data influences the final abundance pattern in different types of  $r$  processes are explored in Refs. [31–33, 35, 36, 38, 39, 44].

Any nucleus with impact parameter above  $F \sim 10$  (purple shading) implies a significant global change to the abundances. Only Palladium ( $_{46}\text{Pd}$ ), Cadmium ( $_{48}\text{Cd}$ ), Indium ( $_{49}\text{In}$ ), and Tin ( $_{50}\text{Sn}$ ) isotopes show sensitivities above  $F = 20$  in our studies. Table 1 includes the  $F$  measures of these most impactful nuclei.

TABLE I: Important nuclei from Fig. 2 with  $F_{max} \geq 20$ .

$Z$	$N$	$A$	$F_{max}$	Trajectory
48	84	132	101.39	high entropy hot
50	86	136	83.68	high entropy hot
49	84	133	74.59	high entropy hot
49	86	135	73.82	high entropy hot
49	85	134	72.84	high entropy hot
49	87	136	71.04	high entropy hot
49	88	137	68.08	high entropy hot
49	89	138	66.43	high entropy hot
48	88	136	58.42	low entropy hot
46	86	132	55.56	nsm
48	86	134	52.38	low entropy hot
46	86	132	48.67	cold
46	84	130	43.73	cold
48	90	138	37.86	low entropy hot
46	85	131	34.81	cold
50	88	138	29.64	high entropy hot
46	84	130	24.19	nsm
48	88	136	24.10	cold
48	85	133	23.38	low entropy hot
48	87	135	21.12	low entropy hot
48	89	137	20.63	cold

#### V. ABUNDANCE PATTERN PREDICTIONS

We now use the above sensitivity study results to examine the variances that can arise in the final abundance pattern due to uncertainties in nuclear masses. In each sensitivity study we first select the nuclei for which  $F \geq 0.1$  as shown in Fig. 2. We create an ensemble of abundance patterns from the simulations that include the individual mass changes  $\pm 0.5$  MeV of these nuclei. We then compute the variance of this reduced ensemble of abundances for each value of  $A$ . The variance in the final abundance patterns for the low entropy hot

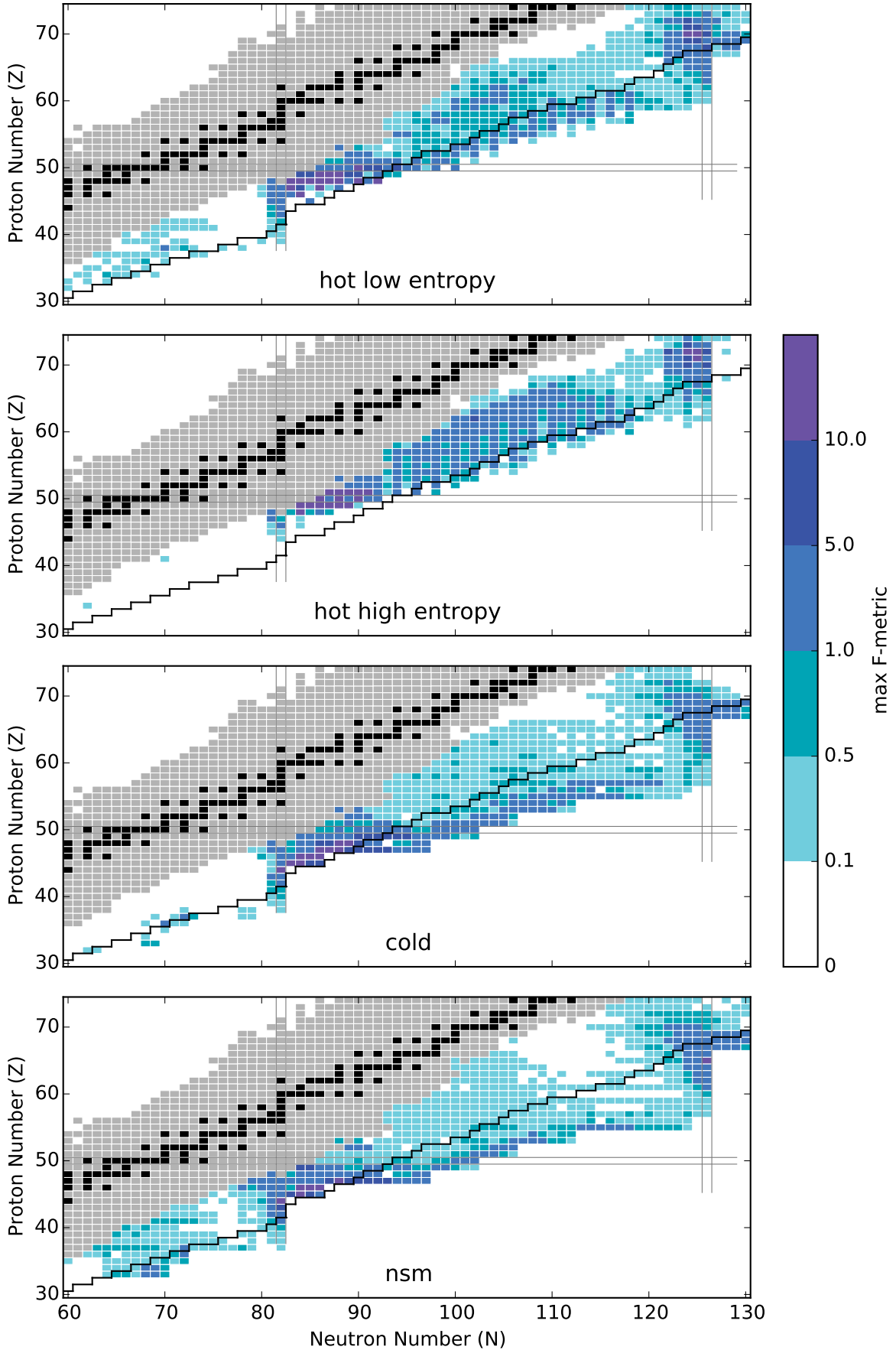


FIG. 2: Nuclei that significantly impact final  $r$ -process abundances for four astrophysical conditions. The intensity of the color denotes the maximum  $F$  value, Eqn. 4, resulting from individual  $\pm 0.5$  MeV mass variations. Light gray denotes the extent of measured masses from the 2012 AME and stable nuclei are colored black. For reference, estimated accessibility limits are shown for the upcoming Facility for Rare Isotope Beams (FRIB) (black line - intensity of  $10^{-4}$  particles per second [63]).

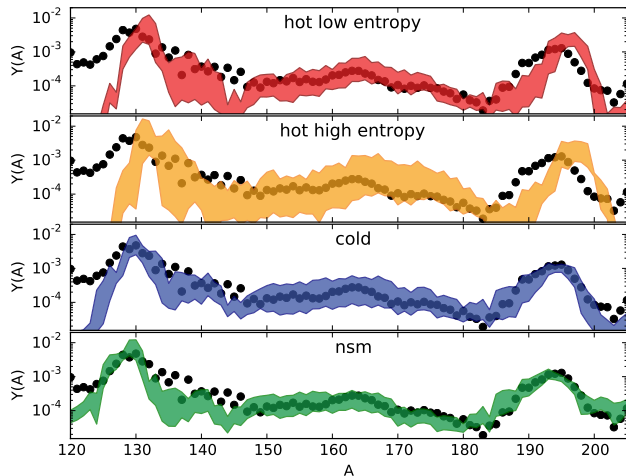


FIG. 3: Variances of the ensembles of final abundance patterns (shaded bands) for the four sensitivity studies described in this work, compared to scaled solar  $r$ -process residuals (black circles) from [64].

wind, high entropy hot wind, cold wind and neutron star merger studies are shown in Fig. 3 compared to the solar isotopic  $r$ -process residuals.

The dependence of  $r$ -process predictions on the uncertainties in nuclear masses is shown by variance bands for four different astrophysical conditions in Fig. 3. These four trajectories have distinct  $r$ -process paths and dynamics during freeze-out which means the variance in abundances in each environment comes from a different aspect of the dependence on nuclear masses as mentioned above. This result is only obtainable by using our approach of consistently propagating uncertainties from nuclear masses to all of the relevant nuclear quantities for the  $r$  process.

One may be tempted to rule out the hot conditions as the variance bands are clearly offset for the third ( $A = 195$ ) peak. However, we note that our approach here actually underestimates these bands *in all scenarios* — larger uncertainties from reaction rate calculations are not included, which are particularly important for the hot scenarios, and mass changes in these studies are done on an individual basis. Methods that rely on a global Monte Carlo approach have the ability to resolve these drawbacks. Preliminary work [29] in this direction suggests details of the abundance pattern can be clearly resolved if mass uncertainties are reduced to less than 0.1 MeV. The next generation of nuclear mass measurement campaigns will be crucial in the progress toward this ambitious goal.

With this caution in mind, Fig. 3 confirms our previous results that mass model uncertainties are currently too large for precision abundance pattern predictions capa-

ble of differentiating between  $r$ -process conditions [44]. For example, the formation of the  $A \sim 160$  rare earth peak can in principle be used to constrain the  $r$ -process site [48], however the variance bands in Fig. 3 are larger than the peak itself. This indicates that the features of the mass surface in this region responsible for rare earth peak formation are likely on the order of the rms value of FRDM2012 or smaller.

We also note that the new FRDM2012 masses show marked improvement over the FRDM1995 masses in matching features from the solar pattern, as is clear from a comparison of the final abundances of Fig. 3 to those in Ref. [44]. The most notable improvement of the mass model comes from an enhanced description of nuclei in the transition region between the  $N \sim 82$  region and the rare earth region.

## VI. CONCLUSION

In summary, we have shown for the first time how uncertainties in *individual* nuclear masses propagate to influence and shape the  $r$ -process abundance distribution across the chart of nuclides. We consider variations of individual nuclear masses and recalculate consistently all relevant  $Q$ -values, neutron capture rates, photodissociation rates,  $\beta$ -decay rates and  $\beta$ -delayed neutron emission probabilities, as shown in Fig. 1. We find mass uncertainties of  $\pm 0.5$  MeV have a significant impact on  $r$ -process abundance predictions as summarized in Fig. 2. In terms of our metric, a value of  $F \sim 20$  represents a large local change or a global shift in  $r$ -process abundances.

We explore changes to masses of  $\pm 0.5$  MeV from FRDM2012 in four astrophysical trajectories: a low entropy hot wind, a high entropy hot wind, a cold wind, and a neutron star merger. Shifts in the equilibrium path play the dominant role in a hot  $r$  process, and our results here mirror earlier studies [36, 38] where mass variations were propagated only to the photodissociation rates. Changes to weak decay properties and neutron capture rates are essential to include particularly in the cold wind and merger cases where photodissociation channel is suppressed. We find a similar dependence on nuclear masses for all astrophysical conditions studied, as shown in Fig. 3, due to the propagation of mass uncertainties to all relevant quantities. The nuclei with the most impactful masses lie along the equilibrium  $r$ -process path, as expected, and also along the decay paths to stability. This result strongly reinforces our conclusions from previous studies that understanding freeze-out is critical for predicting  $r$ -process abundances under any astrophysical conditions.

Many of the influential nuclear masses identified in our studies will be accessible to future radioactive beam facilities. These measurements have the potential to dramatically improve the precision of  $r$ -process simulations. Still, some masses will remain beyond experimental reach. It is

therefore also of key importance to improve global mass models. This work provides additional motivation for strengthening efforts in improving the global description of nuclear masses as it clearly shows that current mass model uncertainties are still too large for the finer details of the isotopic  $r$ -process abundance pattern to be resolved. The question then arises: how well do we need to know nuclear masses in order to predict a final composition of the  $r$  process? Studies which address this question strongly point to the resolution of abundance features if global model uncertainties are reduced to less than 0.1 MeV [29, 44]. Thus, a concerted effort is required by the community to analyze model inputs and

physical assumptions in order to achieve reliable calculations as close to this threshold as possible [65–67].

## VII. ACKNOWLEDGEMENTS

We thank Gail McLaughlin for helpful discussions. This work was supported in part by the National Science Foundation through the Joint Institute for Nuclear Astrophysics grant numbers PHY0822648 and PHY1419765, and the Department of Energy under contract de-sc0013039 (RS).

- 
- [1] E. M. Burbidge, G. R. Burbidge, W. A. Fowler, and F. Hoyle, *Reviews of Modern Physics* **29**, 547 (1957).
- [2] Committee on The Physics of The Universe, Board on Physics and Astronomy, Division on Engineering and Physical Sciences, and National Research Council of The National Academies, *Connecting Quarks with the Cosmos: Eleven Science Questions for the New Century. Committee on the Physics of the Universe. Board on Physics and Astronomy. Division on Engineering and Physical Sciences. NATIONAL RESEARCH COUNCIL OF THE NATIONAL ACADEMIES. Washington D.C.: NATIONAL ACADEMY PRESS, 2003*, Tech. Rep. (2003).
- [3] M. Arnould, S. Goriely, and K. Takahashi, *Physics Reports* **450**, 97 (2007).
- [4] J. M. Lattimer and D. N. Schramm, *Astrophys. J.* **192**, L145 (1974).
- [5] S. Goriely, A. Bauswein, and H.-T. Janka, *Astrophysical Journal Letters* **738**, L32 (2011), arXiv:1107.0899 [astro-ph.SR] .
- [6] O. Korobkin, S. Rosswog, A. Arcones, and C. Winteler, *Monthly Notices of the Royal Astronomical Society* **426**, 1940 (2012), arXiv:1206.2379 [astro-ph.SR] .
- [7] S. Wanajo, Y. Sekiguchi, N. Nishimura, K. Kiuchi, K. Kyutoku, and M. Shibata, *Astrophys. J.* **789**, L39 (2014), arXiv:1402.7317 [astro-ph.SR] .
- [8] O. Just, A. Bauswein, R. A. Pulpillo, S. Goriely, and H.-T. Janka, *MNRAS* **448**, 541 (2015), arXiv:1406.2687 [astro-ph.SR] .
- [9] C. Sneden, J. J. Cowan, and R. Gallino, *Annual Review of Astronomy & Astrophysics* **46**, 241 (2008).
- [10] I. U. Roederer, G. W. Preston, I. B. Thompson, S. A. Shtetman, and C. Sneden, *Astrophys. J.* **784**, 158 (2014), arXiv:1402.4144 [astro-ph.SR] .
- [11] L.-X. Li and B. Paczyński, *Astrophys. J.* **507**, L59 (1998), astro-ph/9807272 .
- [12] L. F. Roberts, D. Kasen, W. H. Lee, and E. Ramirez-Ruiz, *Astrophys. J.* **736**, L21+ (2011), arXiv:1104.5504 [astro-ph.HE] .
- [13] J. Barnes and D. Kasen, *Astrophys. J.* **775**, 18 (2013), arXiv:1303.5787 [astro-ph.HE] .
- [14] E. Berger, W. Fong, and R. Chornock, *ApJ* **774**, L23 (2013), arXiv:1306.3960 [astro-ph.HE] .
- [15] N. R. Tanvir, A. J. Levan, A. S. Fruchter, J. Hjorth, R. A. Hounsell, K. Wiersema, and R. L. Tunnicliffe, *Nature* **500**, 547 (2013), arXiv:1306.4971 [astro-ph.HE] .
- [16] D. Argast, M. Samland, F.-K. Thielemann, and Y.-Z. Qian, *Astron. Astrophys.* **416**, 997 (2004), astro-ph/0309237 .
- [17] Y. Komiya, S. Yamada, T. Suda, and M. Y. Fujimoto, *Astrophys. J.* **783**, 132 (2014), arXiv:1401.6261 [astro-ph.GA] .
- [18] F. Matteucci, D. Romano, A. Arcones, O. Korobkin, and S. Rosswog, *MNRAS* **447**, 326 (2015).
- [19] B. S. Meyer, G. J. Mathews, W. M. Howard, S. E. Woosley, and R. D. Hoffman, *Astrophys. J.* **399**, 656 (1992).
- [20] S. E. Woosley, J. R. Wilson, G. J. Mathews, R. D. Hoffman, and B. S. Meyer, *Astrophys. J.* **433**, 229 (1994).
- [21] L. Hüdepohl, B. Müller, H.-T. Janka, A. Marek, and G. G. Raffelt, *Physical Review Letters* **104**, 251101 (2010), arXiv:0912.0260 [astro-ph.SR] .
- [22] T. Fischer, S. C. Whitehouse, A. Mezzacappa, F.-K. Thielemann, and M. Liebendörfer, *Astronomy and Astrophysics* **517**, A80+ (2010), arXiv:0908.1871 [astro-ph.HE] .
- [23] A. Arcones and F.-K. Thielemann, *Journal of Physics G Nuclear Physics* **40**, 013201 (2013), arXiv:1207.2527 [astro-ph.SR] .
- [24] L. F. Roberts, S. Reddy, and G. Shen, *Phys. Rev. C* **86**, 065803 (2012), arXiv:1205.4066 [astro-ph.HE] .
- [25] C. Winteler, R. Käppeli, A. Perego, A. Arcones, N. Vasset, N. Nishimura, M. Liebendörfer, and F.-K. Thielemann, *Astrophys. J.* **750**, L22 (2012), arXiv:1203.0616 [astro-ph.SR] .
- [26] P. Banerjee, W. C. Haxton, and Y.-Z. Qian, *Phys. Rev. Lett.* **106**, 201104 (2011), arXiv:1103.1193 [astro-ph.SR] .
- [27] K. Nakamura, T. Kajino, G. J. Mathews, S. Sato, and S. Harikae, *International Journal of Modern Physics E* **22**, 1330022 (2013).
- [28] A. Malkus, J. P. Kneller, G. C. McLaughlin, and R. Surman, *Phys. Rev. D* **86**, 085015 (2012), arXiv:1207.6648 [hep-ph] .
- [29] M. Mumpower, R. Surman, and A. Aprahamian, *Capture Gamma Spectroscopy and Related Topics (CGS15)*, to appear in EPJ Web of Conferences (2014).
- [30] M. Mumpower, R. Surman, and A. Aprahamian, *Journal of Physics: Conference Series* **599**, 012031 (2015).
- [31] J. Beun, J. C. Blackmon, W. R. Hix, G. C. McLaugh-



- lin, M. S. Smith, and R. Surman, *Journal of Physics G Nuclear Physics* **36**, 025201 (2009), arXiv:0806.3895 [nucl-th] .
- [32] R. Surman, J. Beun, G. C. McLaughlin, and W. R. Hix, *Phys. Rev. C* **79**, 045809 (2009), arXiv:0806.3753 [nucl-th] .
- [33] M. R. Mumpower, G. C. McLaughlin, and R. Surman, *Phys. Rev. C* **86**, 035803 (2012), arXiv:1204.0437 [nucl-th] .
- [34] R. Surman, M. Mumpower, J. Cass, I. Bentley, A. Aprahamian, and G. C. McLaughlin, in *European Physical Journal Web of Conferences*, European Physical Journal Web of Conferences, Vol. 66 (2014) p. 7024, arXiv:1309.0059 [nucl-th] .
- [35] M. Mumpower, J. Cass, G. Passucci, R. Surman, and A. Aprahamian, *AIP Advances* **4**, 041009 (2014).
- [36] S. Brett, I. Bentley, N. Paul, R. Surman, and A. Aprahamian, *European Physical Journal A* **48**, 184 (2012), arXiv:1211.7310 [nucl-th] .
- [37] R. Surman, M. Mumpower, J. Cass, and A. Aprahamian (2013) arXiv:1309.0058 [nucl-th] .
- [38] A. Aprahamian, I. Bentley, M. Mumpower, and R. Surman, *AIP Advances* **4**, 041101 (2014).
- [39] R. Surman, M. Mumpower, and A. Aprahamian, *Advances in Radioactive Isotope Science (ARIS2014)*, to appear in *JPS Conference Proceedings* (2015).
- [40] T. Suzuki, T. Yoshida, T. Kajino, and T. Otsuka, *Phys. Rev. C* **85**, 015802 (2012), arXiv:1110.3886 [nucl-th] .
- [41] N. Nishimura, T. Kajino, G. J. Mathews, S. Nishimura, and T. Suzuki, *Phys. Rev. C* **85**, 048801 (2012), arXiv:1203.5281 [astro-ph.SR] .
- [42] A. Arcones and G. Martínez-Pinedo, *Phys. Rev. C* **83**, 045809 (2011), arXiv:1008.3890 [astro-ph.SR] .
- [43] M. G. Bertolli, F. Herwig, M. Pignatari, and T. Kawano, *ArXiv e-prints* (2013), arXiv:1310.4578 [astro-ph.SR] .
- [44] M. Mumpower, R. Surman, D. L. Fang, M. Beard, and A. Aprahamian, *Journal of Physics G Nuclear Physics* **42**, 034027 (2015).
- [45] B. S. Meyer, *Physical Review Letters* **89**, 231101 (2002).
- [46] A. Arcones, H.-T. Janka, and L. Scheck, *Astronomy and Astrophysics* **467**, 1227 (2007), astro-ph/0612582 .
- [47] R. Surman, J. Engel, J. R. Bennett, and B. S. Meyer, *Physical Review Letters* **79**, 1809 (1997).
- [48] M. Mumpower, G. McLaughlin, and R. Surman, *ArXiv e-prints* (2012), arXiv:1202.1758 [astro-ph.SR] .
- [49] M. R. Mumpower, G. C. McLaughlin, and R. Surman, *Phys. Rev. C* **85**, 045801 (2012), arXiv:1109.3613 [nucl-th] .
- [50] R. Surman and J. Engel, *Phys. Rev. C* **64**, 035801 (2001), arXiv:nucl-th/0103049 .
- [51] R. Surman, G. C. McLaughlin, M. Ruffert, H. Janka, and W. R. Hix, *ApJ* **679**, L117 (2008), arXiv:0803.1785 .
- [52] J. Beun, G. C. McLaughlin, R. Surman, and W. R. Hix, *Phys. Rev. C* **77**, 035804 (2008), arXiv:0707.4498 .
- [53] K.-L. Kratz, K. Farouqi, and P. Möller, *ApJ* **792**, 6 (2014), arXiv:1406.2529 [astro-ph.SR] .
- [54] W. M., G. Audi, W. A. H., K. F. G., M. MacCormick, X. Xu, and B. Pfeiffer, *Chinese Physics C* **36**, 3 (2012).
- [55] S. Goriely, S. Hilaire, and A. J. Koning, *Astronomy and Astrophysics* **487**, 767 (2008), arXiv:0806.2239 .
- [56] A. Gilbert and A. G. W. Cameron, *Canadian Journal of Physics* **43**, 1446 (1965).
- [57] J. Kopecky and M. Uhl, *Phys. Rev. C* **41**, 1941 (1990).
- [58] “<http://www.nndc.bnl.gov/ensdf/>,” (2015).
- [59] P. Möller, B. Pfeiffer, and K.-L. Kratz, *Phys. Rev. C* **67**, 055802 (2003).
- [60] T. Kawano, P. Möller, and W. B. Wilson, *Phys. Rev. C* **78**, 054601 (2008).
- [61] M. Beard, E. Uberseder, R. Crowter, and M. Wiescher, *Phys. Rev. C* **90**, 034619 (2014).
- [62] M. Thoennessen, *Nuclear Data Sheets* **118**, 85 (2014).
- [63] (2015).
- [64] C. Arlandini, F. Käppeler, K. Wisshak, R. Gallino, M. Lugaro, M. Busso, and O. Straniero, *ApJ* **525**, 886 (1999), arXiv:astro-ph/9906266 .
- [65] O. Bohigas and P. Leboeuf, *Physical Review Letters* **88**, 092502 (2002), nucl-th/0110025 .
- [66] J. Barea, A. Frank, J. G. Hirsch, and P. Van Isacker, *Physical Review Letters* **94**, 102501 (2005), nucl-th/0502038 .
- [67] H. Olofsson, S. Åberg, O. Bohigas, and P. Leboeuf, *Physical Review Letters* **96**, 042502 (2006), nucl-th/0602041 .